DESY 96-035
hep-ph/9602418
Februar 1996

ISSN 0418-9833

Inclusive One– and Two–Jet Cross Sections in $\gamma\gamma$ Reactions at e^+e^- Colliders

T. Kleinwort, G. Kramer
II. Institut für Theoretische Physik*
Universität Hamburg
D - 22761 Hamburg, Germany

Abstract

We have calculated inclusive one– and two–jet production in photon–photon collisions superimposing direct, single resolved and double resolved cross sections for center of mass energies of the LEP1, LEP2 and NLC range. The direct and single resolved cross sections are calculated up to next–to–leading order. The double resolved two–jet cross section is calculated only in LO with a k factor estimated from the NLO one–jet cross section. Various differential cross sections as functions of transverse momenta and rapidities of the jets are evaluated.

*Supported by Bundesministerium für Forschung und Technologie, Bonn, Germany under Contract 05 6HH93P(5) and EEC Program "Human Capital and Mobility" through Network "Physics at High Energy Colliders" under Contract CHRX–CT93–0357 (DG12 COMA)

1 Introduction

In a recent paper we presented theoretical results for the production of high–p_T jets in almost–real photon–photon collisions [1] and compared them with recent experimental data for inclusive one– and two–jet cross sections from the two TRISTAN collaborations, TOPAZ [2] and AMY [3]. Due to the increased c.m. energy of the TRISTAN ring as compared to earlier low energy experiments at PETRA and PEP the TOPAZ and AMY cross sections extend to transverse momenta of up to 8 GeV. It is hoped that coming data from $\gamma\gamma$ collisions at LEP1 and particularly from LEP2 will enlarge the p_T range further. Production of high–p_T jets probes the short–distance dynamics of photon–photon reactions. In addition to providing tests of perturbative QCD, data from $\gamma\gamma$ reactions give us information on the photon structure function.

In leading order QCD (LO) three distinct classes of contributions to the cross section [4] are identified: (i) The direct contribution, in which the two photons couple directly to quarks and neither of the photons is resolved into its partonic constituents (DD component in the following). (ii) The single–resolved contribution, where one of the photons interacts with the partonic constituents of the other (DR component). (iii) The double–resolved contribution, where both photons are resolved into partonic constituents before the hard scattering process takes place (RR component). In the DD component we have only the two high–p_T jets in the final state and no additional spectator jets. In the DR case one spectator jet coming from low transverse momentum fragments of one of the photons is present and in the RR component we have two such spectator or photon remnant jets. Experimental separation of the three classes is in principle possible and depends whether the experimental arrangements allow to tag the spectator jets.

In next–to–leading order QCD (NLO) the photon–quark collinear singularity arising in the DD and DR components is subtracted and absorbed into the photon structure function in accord with the factorization theorem. This subtraction procedure at the factorization scale M introduces an interdependence of the three components so that a unique separation into DD, DR and RR classes is not possible anymore. This means that in NLO all three components must be considered together and consistently be calculated up to NLO in the photon structure functions [5, 6] and in the hard scattering cross sections.

The photon structure functions are inherently non-perturbative quantities whose magnitude and dependence on the fractional momentum x of the outgoing parton must be measured at a reference scale ${M_0}^2$. The change with M^2 is obtained from perturbative QCD evolution equations.

Complete NLO calculations for high–p_T jet production in $\gamma\gamma$ reactions have been done previously for the inclusive single jet cross section [1, 7] and compared to experimental data from TRISTAN [2, 3]. The double resolved contribution to the NLO single jet inclusive cross section has been investigated in [8] for TRISTAN, LEP1 and LEP2 energies in order to study the dependence on the photon structure function. The restriction to the RR contribution was motivated in [8] that by tagging the two spectator jets it could be isolated experimentally from the other components. Unfortunately this is possible only in LO since NLO corrections to the DD and DR components can produce spectator jets due to the separation of singularities with the help of kinematic constraints.

In our previous work [1] we also calculated the complete NLO inclusive dijet cross sections for the DD and DR contributions and estimated the RR contribution by a LO calculation with k factors taken from the NLO inclusive single–jet cross section. This was justified since at TRISTAN energies, for which the calculation was done, the RR cross section contributes only a

small fraction of the total sum in the high–p_T region. In this paper we extend these calculations to LEP1, LEP2 and NLC collider energies. Although at these higher energies and at moderate p_T the double resolved cross section is much more important, we expect that the estimate of the RR dijet cross sections with a k factor will still be reliable. In addition we shall present complete NLO predictions for the single–jet inclusive cross section at these energies which we expect to be measured first. Since in our earlier work where we compared also to experimental dijet cross sections measured by TOPAZ and AMY no details for the calculation of the cross sections were given, we shall present them in this longer paper.

The outline of the rest of the paper is as follows. In section 2 we first give the DD cross section in leading order also to fix the notation. Then we present the details of the next–to–leading order calculation for the DD two–jet cross section in section 3.

The calculation of the DR and RR cross sections is based on the work of [10] and [11]. In [10] the formalism for inclusive one– and two–jet cross sections is worked out and applied to the calculation of the direct process on jet production in low Q^2 ep collisions. In [11] the inclusive one–jet cross section for ep collisions with a resolved photon was calculated which can easily be applied to the RR cross section in $\gamma\gamma$ reactions.

The numerical results for the DD, DR and RR one– and two–jet cross sections are given in section 4. In section 5 we summarize our results and draw some conclusions.

2 Leading Order Cross Section

2.1 Photon Spectrum

The cross sections which we have computed are for kinematical conditions as we expect them for $\gamma\gamma$ collisions at LEP1, LEP2 and the NLC. For LEP1 and LEP2 the spectrum of the virtual photons is described in the Weizsäcker–Williams approximation (WWA) by the formula [12]

$$\begin{aligned} F_{\gamma/e}(x_a) &= \frac{\alpha}{2\pi}\left\{\frac{1+(1-x_a)^2}{x_a}\ln\frac{E^2\Theta_c^2(1-x_a)^2+m_e^2x_a^2}{m_e^2x_a^2}\right. \\ &\left. +2(1-x_a)\left[\frac{m_e^2x_a}{E^2\Theta_c^2(1-x_a)^2+m_e^2x_a^2}-\frac{1}{x_a}\right]\right\}, \end{aligned} \tag{1}$$

where m_e is the electron mass and $x_a = (q_a k_b)/(k_b k_a) \simeq E_\gamma/E$ is the fraction of the initial positron energy transferred to the photon with E being the beam energy of the incoming positrons and electrons, respectively. $k_a(k_b)$ is the four momentum of the incoming positron (electron) and $q_a = k_a - k_a'$ is the four momentum of the virtual photon emitted by the positron. The momentum fraction on the electron side is denoted as x_b with $x_b = (k_a q_b)/(k_a k_b)$ and $q_b = k_b - k_b'$.

In the equivalent photon approximation, the cross section for $e^+ + e^- \to e^+ + e^- + X$ with arbitrary final state X is then given by the convolution

$$\mathrm{d}\sigma\left(e^+ + e^- \to e^+ + e^- + X\right) = \int\limits_{x_{a,\min}}^{1} \mathrm{d}x_a \int\limits_{x_{b,\min}}^{1} \mathrm{d}x_b\, F_{\gamma_a/e}(x_a) F_{\gamma_b/e}(x_b)\, \mathrm{d}\sigma(\gamma_a\gamma_b \to X), \tag{2}$$

where $\mathrm{d}\sigma(\gamma_a\gamma_b \to X)$ denotes the cross section for $\gamma_a\gamma_b \to X$ with real photons of energies $E_{\gamma_a} = x_a E$ and $E_{\gamma_b} = x_b E$, respectively.

The LEP1 cross sections are calculated with $\sqrt{S} = 2E = 90\,GeV$. The angle Θ_c is the maximum angle under which the positrons (electrons) are tagged, which we assume $\Theta_c = 3.0°$. For the LEP2 cross section we have chosen $\sqrt{S} = 175\,GeV$ and $\Theta_c = 30\,mrad$. For the NLC collider option the photon spectra will be specified later when we present our results.

2.2 Jet Cross Sections in LO

In this section we write down the leading order cross section for the production of jets with two direct photons, i.e. the DD cross section in LO. This is given by the differential cross section for two–jet production in the quark parton model, i.e. the cross section for $\gamma_a\gamma_b \to q\bar{q}$, which must be convoluted with the photon distribution functions according to (2).

The final state quark (antiquark) has momentum $p_1(p_2)$ which can be expressed by their transverse momentum p_T and rapidities η_1 and η_2. The convention is that the z direction is parallel to the electron beam direction. From energy and momentum conservation one obtains

$$x_a = \frac{p_T}{2E}\left(e^{-\eta_1} + e^{-\eta_2}\right) \tag{3}$$

$$x_b = \frac{p_T}{2E}\left(e^{\eta_1} + e^{\eta_2}\right). \tag{4}$$

Thus, the kinematical variables of the two jets are related to the scaling variables x_a and x_b. Under the actual experimental conditions x_a and x_b are restricted to fixed intervals, $x_{\min} < x_a, x_b < x_{\max} < 1$. We shall disregard these constraints and allow x_a and x_b to vary in the kinematically allowed range $x_{a,b,\min} < x_a, x_b < 1$, where

$$x_{a,\min} = \frac{p_T e^{-\eta_1}}{2E - p_T e^{\eta_1}} \tag{5}$$

and a similar equation for $x_{b,\min}$. From eq. (3) and (4), we can express x_b as a function of p_T, η_1 and x_a:

$$x_b = \frac{x_a p_T e^{\eta_1}}{2x_a E - p_T e^{-\eta_1}}. \tag{6}$$

Depending on x_a, different regions of the photon energy x_b contribute. Whereas for fixed x_a and x_b, i.e. fixed energies for both photons, η_1 and η_2 are fully determined by p_T (up to sign ambiguities), η_1 and η_2 are allowed to vary due to the kinematical range of the photon energies in the intervals $x_{a,b} \in [x_{a,b,\min}, 1]$. $x_{a,b,\min}$ are obtained from (5) and are equal to ${p_T}^2/E^2$.

The two–jet cross section for $e^+ + e^- \to e^+ + e^- + \mathrm{jet}_1 + \mathrm{jet}_2$ is obtained from

$$\frac{\mathrm{d}^3\sigma}{\mathrm{d}p_T \mathrm{d}\eta_1 \mathrm{d}\eta_2} = x_a F_{\gamma_a/e}(x_a) x_b F_{\gamma_b/e}(x_b) \frac{\mathrm{d}\sigma}{dt}\left(\gamma_a\gamma_b \to p_1 p_2\right). \tag{7}$$

$\dfrac{\mathrm{d}\sigma}{dt}$ stands for the differential cross section of the process $\gamma_a\gamma_b \to p_1 p_2$. The invariants of this process are $s = (q_a + q_b)^2$, $t = (q_b - p_1)^2$ and $u = (q_b - p_2)^2$. They are expressed by the final state variables p_T, η_1 and η_2 and the initial state momentum fractions x_a and x_b:

$$s = 4x_a x_b E^2 \tag{8}$$

$$t = -2x_a E p_T e^{\eta_2} = -2x_b E p_T e^{-\eta_1} \tag{9}$$

$$u = -2x_a E p_T e^{\eta_1} = -2x_b E p_T e^{-\eta_2}. \tag{10}$$

So, the dependence of the two–jet cross section on p_T, η_1 and η_2 is determined through the two photon distribution functions and the cross section for the $\gamma\gamma$ subprocess, which depends on s, t and u.

For the inclusive one–jet cross section, we must integrate over one of the rapidities in (7). We integrate over η_2 and transform to the variable x_a using (3). The result is the cross section for $e^+ + e^- \to e^+ + e^- + \text{jet} + X$, which depends on p_T and η:

$$\frac{\mathrm{d}^2\sigma}{\mathrm{d}p_T \mathrm{d}\eta} = \int\limits_{x_{a\,\min}}^{1} \mathrm{d}x_a x_a F_{\gamma_a/e}(x_a) F_{\gamma_b/e}(x_b) \frac{4Ep_T}{2x_aE - p_Te^{-\eta}} \frac{\mathrm{d}\sigma}{\mathrm{d}t}(\gamma_a\gamma_b \to p_1p_2)\,. \tag{11}$$

Here, x_b is given by (6) with $\eta_1 = \eta$.

The cross section for the subprocess $\gamma_a\gamma_b \to q_i\bar{q}_i$ is well known and is given by

$$\frac{\mathrm{d}\sigma}{\mathrm{d}t}(\gamma_a\gamma_b \to q_i\bar{q}_i) = \frac{2\pi\alpha^2}{s^2} N_C Q_i^4 \left(\frac{u}{t} + \frac{t}{u}\right) \tag{12}$$

The index i denotes the quark flavour and Q_i the quark charge. N_C is the number of colours. All quarks are considered massless.

3 Next–To–Leading Order Cross Sections

The next–to–leading order corrections are calculated with the help of dimensional regularization. In the following subsections we shall consider the virtual and the real corrections needed to obtain a finite cross section for the DD case in the limit $n \to 4$.

3.1 Virtual Corrections up to $\mathrm{O}(\alpha^2\alpha_s)$

The one loop diagrams for $\gamma\gamma \to q\bar{q}$ have an additional virtual gluon, which leads to an extra factor α_s. These diagrams must be multiplied with the LO diagrams to produce the virtual corrections to the $2 \to 2$ cross section up to $\mathrm{O}(\alpha^2\alpha_s)$. These corrections are well known for many years now [9, 13]. The result can also be obtained from the virtual correction for $\gamma q \to gq$ [10] by taking only the diagrams without the three gluon vertex and substituting the appropriate colour factors. The result can be written as

$$H_V(\gamma\gamma \to q_i\bar{q}_i) = e^4 Q_i^4 \mu^{4\epsilon} \left(\frac{4\pi\mu^2}{s}\right)^{\epsilon} \frac{\alpha_s}{2\pi} \frac{\Gamma(1-\epsilon)}{\Gamma(1-2\epsilon)} 2N_C C_F V_\gamma(s,t,u) + O(\epsilon). \tag{13}$$

H_V gives the virtual correction to the corresponding reactions up to the n–dimensional phase space factor

$$\frac{\mathrm{dPS}^{(2)}}{\mathrm{d}t} = \frac{1}{\Gamma(1-\epsilon)} \left(\frac{4\pi s}{ut}\right)^{\epsilon} \frac{1}{8\pi s} \tag{14}$$

and the flux factor $1/(2s)$. The expression for $V_\gamma(s,t,u)$ can be found in appendix A. The singular terms $\propto 1/\epsilon^2$ and $1/\epsilon$ are proportional to the LO cross section

$$T_\gamma^{(\epsilon)} = (1-\epsilon)\left[\left(\frac{t}{u} + \frac{u}{t}\right)(1-\epsilon) - 2\epsilon\right] \tag{15}$$

with $\epsilon = (4-n)/2$.

3.2 Real Corrections up to $O(\alpha^2\alpha_s)$

For the $2 \to 3$ contributions up to $O(\alpha^2\alpha_s)$, we have to take into account all diagrams with an additional gluon in the final state. The diagrams are shown in Fig. 1.

The four–vectors of these subprocesses will be labeled by $q_a q_b \to p_1 p_2 p_3$. The invariants will be denoted by $s_{ij} = (p_i + p_j)^2$, $(i, j = a, b, 1, 2, 3)$. For massless partons, the $2 \to 3$ contributions contain singularities at $s_{ij} = 0$. They can be extracted with the dimensional regularization method and can be cancelled against those which originate from the one–loop contributions or are absorbed in the renormalized photon structure functions.

To achieve this, we go through the same steps as described for example in [10]. First, we calculated the $2 \to 3$ subprocesses in n dimensions. In our case we have two classes of singularities. Examples of these are shown in Fig. 2. The X marks the propagator leading to the divergence. In the first graph, the vanishing of the invariant s_{12} leads to a final state singularity and the second graph becomes singular for $s_{b3} = 0$, which then leads to an initial state singularity.

When squaring the sum of all diagrams in Fig. 2, we encounter terms where more than one of the invariants become singular, e.g. when the gluon momentum $p_1 \to 0$, so that $s_{12} = 0$ and $s_{13} = 0$. These infrared singularities are disentangled by a partial fractioning decomposition, so that every term has only one vanishing denominator. Non–singular terms are discarded. It turns out that in this limit the results are always proportional to the LO cross sections involved in the hard scattering, namely T_γ and T_q, where T_q stands for $\gamma q \to gq$, so that they can be written as

$$H_{F,I} \;=\; K_{F,I} T_{\gamma,q}. \tag{16}$$

Here F and I denote the contributions originating from the final(F) and initial(I) state singularities, respectively.

The last step is to integrate the decomposed matrix elements analytically in the region $s_{ij} \leq ys$, where y is the upper bound for the integration and has to be chosen small enough so that it is justified to neglect terms of $O(y)$, which was assumed already in the partial fractioning above. This means we use an invariant mass cut to separate the genuine $2 \to 3$ contributions from the $2 \to 2$ contributions. For the terms with final state singularities y determines the phase space region where two partons, i.e. a quark and a gluon, are combined in one jet. In the case of initial state singularities y determines the boundary between the remnant jet of the photon and the $2 \to 2$ hard scattering $\gamma q \to gq$. In [9] the separation of the final state singularities was done with the Sterman–Weinberg parameters ε and δ, where ε is the cut on the gluon energy and δ measures the angle between the momenta of the quark and the gluon in the recombination of a quark and a gluon into one jet. The integration produces terms $\propto 1/\epsilon^2$ and $1/\epsilon$, which cancel against those in the virtual corrections or be absorbed into the photon structure functions. In the following we shall give the results for the final and the initial state singularities separately.

3.2.1 Final State Singularities

In this subsection, we assume that after partial fractioning the $2 \to 3$ matrix elements are singular only for $s_{12} = 0$. For the integration over the singular phase space region we choose as coordinate system the c.m. system of the partons p_1 and p_2. The angles of the other parton three–momenta q_a and p_3 with respect to p_1 and p_2 are shown in Fig. 3. χ is the angle between

the momenta q_a and p_3, θ is the angle between q_a and p_1, and ϕ is the azimuthal angle between the planes defined by q_a and p_1 and p_a and p_3, respectively. Instead of θ we also use the variable

$$b = \frac{1}{2}(1-\cos\theta). \tag{17}$$

The angle ϕ can be integrated out easily, because the matrix elements do not depend on it in the limit that non–singular terms are discarded.

Here, we define the invariants

$$s = (q_a+q_b)^2 \tag{18}$$
$$t = (q_b-p_1-p_2)^2 - 2p_1p_2 \tag{19}$$
$$u = (q_b-p_3)^2 \tag{20}$$

which differ from the corresponding two-body invariants, but are equal to them for $p_1 = 0$ or p_2 collinear with p_1. The variable to be integrated is

$$z' = \frac{p_1.p_2}{q_a.q_b}. \tag{21}$$

The three–body phase space in n dimensions can be factorized into

$$\mathrm{dPS}^{(3)} = \mathrm{dPS}^{(2)}\mathrm{dPS}^{(r)}, \tag{22}$$

where

$$\frac{\mathrm{dPS}^{(2)}}{\mathrm{d}t} = \frac{1}{\Gamma(1-\epsilon)}\left(\frac{4\pi s}{tu}\right)^{\epsilon}\frac{1}{8\pi s} \tag{23}$$

and

$$\mathrm{dPS}^{(r)} = \left(\frac{4\pi}{s}\right)^{\epsilon}\frac{\Gamma(1-\epsilon)}{\Gamma(1-2\epsilon)}\frac{s}{16\pi^2}\frac{1}{1-2\epsilon}\mathrm{d}\mu_F \tag{24}$$

with

$$\mathrm{d}\mu_F = \mathrm{d}z' z'^{-\epsilon}\left(1+\frac{z's}{t}\right)^{-\epsilon}\frac{\mathrm{d}b}{N_b}b^{-\epsilon}(1-b)^{-\epsilon}\frac{\mathrm{d}\phi}{N_\phi}\sin^{-2\epsilon}\phi. \tag{25}$$

N_b and N_ϕ are normalization factors:

$$N_b = \int_0^1 \mathrm{d}b\, b^{-\epsilon}(1-b)^{-\epsilon} = \frac{\Gamma^2(1-\epsilon)}{\Gamma(2-2\epsilon)} \tag{26}$$

$$N_\phi = \int_0^\pi \mathrm{d}\phi \sin^{-2\epsilon}\phi = 4^\epsilon\pi\frac{\Gamma(1-2\epsilon)}{\Gamma^2(1-\epsilon)}. \tag{27}$$

The full range of integration is given by $z' \in [0,-t/s]$, $b\in[0,1]$ and $\phi\in[0,\pi]$. The singular region is defined by the requirement that partons p_1 and p_2 are recombined, which means $s_{12}\to 0$. We integrate over this region analytically up to $s_{12}\le ys$, which restricts the range of integration to $0\le z'\le \min\{-t/s, y\}\equiv y_F$.

In the $\gamma\gamma$ case we obtain the final state matrix element in the following form

$$\int \mathrm{dPS}^{(r)} H_F = Q_i^4\mu^{4\epsilon}\left(\frac{4\pi\mu^2}{s}\right)^{\epsilon}\frac{\alpha_s}{2\pi}\frac{\Gamma(1-\epsilon)}{\Gamma(1-2\epsilon)}2N_C C_F F_\gamma(s,t,u) + O(\epsilon). \tag{28}$$

The factor $F_\gamma(s,t,u)$ can be found in Appendix B. It contains infrared and collinear singularities, which cancel against those in the virtual corrections.

3.2.2 Initial State Singularities

Here we integrate over the singularity $s_{b3} = 0$, we use the same p_1–p_2 c.m. system as in the last section. In this case, the outgoing quark p_3 is collinear to the incoming photon momentum q_b. So it becomes part of the photon remnant and p_1 and p_2 are the momenta of the final state in the 2–body subprocess. We introduce the new variable

$$z_b = \frac{p_1 p_2}{q_a q_b} \in [X_b, 1], \tag{29}$$

where $X_b = (p_1 p_2)/(q_a k_b) \simeq E_q/E$ is the fraction of the initial electron energy transferred to the quark.

We have now the following definition for the Mandelstam variables

$$s = (q_a + z_b q_b)^2 \tag{30}$$
$$t = (q_a - p_1)^2 \tag{31}$$
$$u = (q_a - p_2)^2 \tag{32}$$

and the variable, which parametrizes the singular region, is now

$$z'' = \frac{q_b p_3}{q_a q_b}. \tag{33}$$

Again the three–body phase space factorizes into

$$\mathrm{dPS}^{(3)} = \mathrm{dPS}^{(2)} \mathrm{dPS}^{(r)}, \tag{34}$$

where $\mathrm{dPS}^{(2)}$ is again the phase space of the $2 \to 2$ process now in the limit $q_b p_3 \to 0$ given by (23), and

$$\mathrm{dPS}^{(r)} = \left(\frac{4\pi}{s}\right)^{\epsilon} \frac{\Gamma(1-\epsilon)}{\Gamma(1-2\epsilon)} \frac{s}{16\pi^2} H_b(z'') \mathrm{d}\mu_I, \tag{35}$$

where

$$\mathrm{d}\mu_I = \mathrm{d}z'' z''^{-\epsilon} \frac{\mathrm{d}z_b}{z_b} \left(\frac{z_b}{1-z_b}\right)^{\epsilon} \frac{\mathrm{d}\phi}{N_\phi} \sin^{-2\epsilon}\phi \frac{\Gamma(1-2\epsilon)}{\Gamma^2(1-\epsilon)} \tag{36}$$

and

$$H_a(z'') = \left(1 + \frac{z''}{z_a}\right)^{-1+2\epsilon} \left(1 - \frac{z''}{1-z_a}\right)^{-\epsilon} = 1 + O(z'') \tag{37}$$

can be approximated by 1, because it leads only to negligible terms of $O(y)$. The full region of integration is given by $z'' \in [0, -u/s]$, $z_b \in [X_b, 1]$ and $\phi \in [0, \pi]$, where again the dependence on ϕ can easily be integrated out. The singular region where the integration is done analytically is given by the requirement $0 \le z'' \le \min\{-u/s, y\} \equiv y_I$.

The result is

$$\int \mathrm{dPS}^{(r)} H_I = \int_{X_b}^{1} \frac{\mathrm{d}z_b}{z_b} Q_i^4 \mu^{4\epsilon} \left(\frac{4\pi\mu^2}{s}\right)^{\epsilon} \frac{\alpha_s}{2\pi} \frac{\Gamma(1-\epsilon)}{\Gamma(1-2\epsilon)} N_C C_F I_\gamma(z_b; s, t, u) + O(\epsilon). \tag{38}$$

Again, $I_\gamma(z;s,t,u)$ can be found in the appendix.

In the case of initial state singularities the following quark-photon matrix element factorizes

$$T_q^{(\epsilon)}(s,t,u) \;=\; (1-\epsilon)\left[\left(-\frac{t}{s}-\frac{s}{t}\right)(1-\epsilon)+2\epsilon\right]. \tag{39}$$

The case $z'' = q_a p_3/q_a q_b \to 0$ leads to the same result with $(z_b \leftrightarrow z_a)$. The term I_γ shows explicitly the pole in $1/\epsilon$ proportional to

$$P_{q\leftarrow\gamma}(z) \;=\; N_C Q_i^2\left[2z^2-2z+1\right]. \tag{40}$$

This function appears in the evolution equation of the photon structure function as an inhomogeneous or so–called point–like term. Therefore, the photon initial state singularities can be absorbed into the photon structure function.

3.3 DD Jet Cross Section in NLO

To obtain a finite cross section for the DD case, we must add the parts considered in section 3.1 and 3.2. Then the poles in $1/\epsilon$ and $1/\epsilon^2$ cancel and we can take the limit $\epsilon \to 0$. The result is a special kind of two–jet cross section, where the recombination of two partons into one jet or the recombination of a parton with the photon remnant jet is done with an invariant mass cut-off y. Including the NLO corrections, we get

$$\begin{aligned}\frac{\mathrm{d}^3\sigma}{\mathrm{d}p_T\mathrm{d}\eta_1\mathrm{d}\eta_2} \;=\;& x_a F_{\gamma_a/e}(x_a) x_b F_{\gamma_b/e}(x_b)\left[\frac{\mathrm{d}\sigma}{\mathrm{d}t}(\gamma_a\gamma_b\to p_1p_2)\right.\\ &\left.+\frac{\mathrm{d}\tilde\sigma}{\mathrm{d}t}(\gamma_a q\to p_1p_2)+\frac{\mathrm{d}\tilde\sigma}{\mathrm{d}t}(q\gamma_b\to p_1p_2)\right].\end{aligned} \tag{41}$$

In (41), $\dfrac{\mathrm{d}\sigma}{\mathrm{d}t}(\gamma_a\gamma_b\to p_1p_2)$ stands for the two–body contribution in LO and NLO together with analytically integrated contributions of the soft and collinear divergent regions of the three–parton final state. The contributions from the initial state singularities are denoted $\dfrac{\mathrm{d}\tilde\sigma}{\mathrm{d}t}(\gamma_a q\to p_1p_2)$ and $\dfrac{\mathrm{d}\tilde\sigma}{\mathrm{d}t}(q\gamma_b\to p_1p_2)$, where either the photon γ_b or γ_a has collinear singular terms removed, respectively.

The two–body contribution can be written as

$$\frac{\mathrm{d}\sigma}{\mathrm{d}t}(\gamma_a\gamma_b\to p_1p_2) \;=\; CT_\gamma+\frac{\alpha_s^2(\mu^2)}{2\pi}C(T_\gamma A_\gamma+B_\gamma), \tag{42}$$

where

$$A_\gamma \;=\; C_F\left[\frac{2}{3}\pi^2+\ln^2\frac{-t}{s}+\ln^2\frac{-u}{s}-2\ln^2 y_F-3\ln y_F\right] \tag{43}$$

$$\begin{aligned}B_\gamma \;=\;& C_F\left[2\ln\frac{-t}{s}+2\ln\frac{-u}{s}+3\frac{u}{t}\ln\frac{-t}{s}+3\frac{t}{u}\ln\frac{-u}{s}\right.\\ &\left.+\left(2+\frac{u}{t}\right)\ln^2\frac{-u}{s}+\left(2+\frac{t}{u}\right)\ln^2\frac{-t}{s}\right],\end{aligned} \tag{44}$$

$$T_\gamma \;=\; \left(\frac{u}{t}+\frac{t}{u}\right),\ \text{and}\ C=\frac{2\pi\alpha^2}{s^2}Q_i^4N_C. \tag{45}$$

The cut dependence of the final state corrections in A_γ is contained in the y_F dependent terms. For $y_F \to 0$, these terms behave like $(-\ln^2 y_F)$, which leads to unphysical negative cross sections for very small y_F. Thus if y is used as a physical cut, it must be sufficiently large. In most applications, we shall use these results for computing inclusive cross sections, in which the y dependence of the two–jet cross section cancels against the y dependence of the numerically calculated three–jet cross section.

The two–jet cross section for the initial state is calculated from

$$\begin{aligned}
\frac{\mathrm{d}\tilde{\sigma}}{\mathrm{d}t}(q\gamma_b \to p_1 p_2) &= \frac{\mathrm{d}\hat{\sigma}}{\mathrm{d}t}(q\gamma_b \to p_1 p_2)\frac{\alpha}{2\pi} \\
&\quad \int\limits_{X_a}^{1} \frac{\mathrm{d}z_a}{z_a}\left[P_{q\leftarrow\gamma}(z_a)\left(\ln\left(\frac{(1-z_a)y_I s}{z_a M_a^2}\right)-1\right)+N_C Q_i^2\right] \qquad (46) \\
\frac{\mathrm{d}\tilde{\sigma}}{\mathrm{d}t}(\gamma_a q \to p_1 p_2) &= \frac{\mathrm{d}\hat{\sigma}}{\mathrm{d}t}(\gamma_a q \to p_1 p_2)\frac{\alpha}{2\pi} \\
&\quad \int\limits_{X_b}^{1} \frac{\mathrm{d}z_b}{z_b}\left[P_{q\leftarrow\gamma}(z_b)\left(\ln\left(\frac{(1-z_b)y_I s}{z_b M_b^2}\right)-1\right)+N_C Q_i^2\right]. \qquad (47)
\end{aligned}$$

In (46) and (47), M_a resp. M_b are the factorization scales. The dependence on M_a resp. M_b must cancel against the M_a resp. M_b dependences of the LO DR and RD contributions. The cross section $\dfrac{\mathrm{d}\hat{\sigma}}{\mathrm{d}t}$ has the following form

$$\frac{\mathrm{d}\hat{\sigma}}{\mathrm{d}t}(\gamma q \to q g) = \frac{2\pi\alpha\alpha_s}{s^2} Q_i^2 C_F\left(-\frac{s}{t}-\frac{t}{s}\right). \qquad (48)$$

All the results of this section are for the $\overline{\mathrm{MS}}$ subtraction and renormalization scheme.

4 Inclusive One– and Two–Jet Cross Sections

In this section we present some characteristic numerical results for one– and two–jet inclusive cross sections which have been obtained with our method of slicing the phase space with invariant mass cuts. In a short communication we used this method to calculate the differential one– and two–jet cross section as a function of p_T integrated over special rapidity intervals and compared it to recent experimental data of the TOPAZ [2] and AMY [3] collaborations at TRISTAN. For this paper we have calculated various one– and two–jet distributions without applying special cuts on kinematical variables of the initial or final state dictated by the experimental analysis, although our approach is particularly suitable for this.

The calculation of the cross sections proceeds as follows. For the DD and DR components we use the phase space slicing method for the inclusive one– and two–jet cross sections. The details for the calculation of the DD component below the cut are described in the previous section. The DR component is identical with the work in [10] for the direct photoproduction of jets in low Q^2 ep collisions. We must replace the proton structure function by the photon structure function and obtain the cross sections for the single–resolved contribution. With the results presented in [10] and in the previous section we are able to calculate the inclusive cross section for one– and two–jet production. For the double–resolved contribution the NLO corrections for the two–jet cross section are not available yet. Here only the LO cross sections are at our disposal. To estimate the NLO corrections we make use of the NLO cross sections

for the inclusive one–jet case. This cross section has the same structure as the NLO resolved inclusive one–jet cross section for photoproduction $\gamma p \to \text{jet} + X$, where the photon structure function at one vertex is replaced by the proton structure function. For this cross section the NLO corrections are known from earlier work [11]. We use these results and transform the cross section to the γ case by replacing the proton structure function by the photon structure function. This gives us the full NLO inclusive one–jet cross section for which we present results later. We compare the NLO cross section with the RR LO cross section and calculate the k factor from it. Then the same k factor is applied to the LO two–jet cross section. We checked this procedure with the DD and DR cross sections, where we know also the NLO two–jet cross sections. For these cases we found that the k factors for the one– and two–jet cross sections are approximately equal. It is reasonable to expect this also to be the case for the RR cross sections.

The further calculation of the DD and DR cross sections is based on two separate contributions — a set of two–body contributions and a set of three–body contributions. Each set is completely finite, as all singularities have been cancelled or absorbed into structure functions. Each part depends separately on the cut–off y. If y is chosen large enough, the two parts determine physically well defined two–jet and three–jet cross sections. However, our analytic calculations are valid only for very small y, since terms $O(y)$ have been neglected in the analytic integrations. For very small y, the two cross sections have no physical meaning. In this case, the $(\ln y)$ terms force the two–body contributions to become negative, whereas the three–body cross sections are large and positive. When both contributions are added to yield a suitable inclusive cross section, as for example the inclusive one–jet cross section, the dependence on the cut–off y will cancel. Then, the separation of the two y dependent contributions is only a technical device. The cut–off only serves to distinguish the phase space regions, where the integrations are done analytically, from those where they are performed numerically. Furthermore, y must be chosen sufficiently small so that experimental cuts imposed on kinematical variables of the final state do not interfere with the cancellation of the y dependence.

First we consider the inclusive one–jet cross section. We choose the definition of the Snowmass meeting [14] for combining two nearly collinear partons. According to this definition, two partons i and j are recombined if $R_{i,j} < R$ where $R_i = \sqrt{(\eta_i - \eta_J)^2 + (\phi_i - \phi_J)^2}$ is the distance between parton i and jet J in the rapidity–azimuthal space. η_i, ϕ_i and η_J, ϕ_J are the rapidities and the azimuthal angles of parton i and of the recombined jet J, respectively. We choose $R = 1$ in all the following results. The Snowmass condition means that two partons are considered as two separate jets or as a single jet depending whether they lie outside or inside the cone with radius R around the jet momentum. Unfortunately this definition is not unique. In some cases it may happen that two partons i and j qualify both as two individual jets i and j and as a recombined jet ij. In this case we count only the combined jet following [15]. In NLO the final state may consist of two or three jets. The three–jet sample consists of all three-body contributions, which do not fulfill the cone condition. The inclusive cross section will depend on the value of R chosen. It will increase with increasing R.

Before we calculate the final results to be presented in the figures we have made some checks of the NLO corrections to the one– and two–jet cross sections. First we checked that the DD and DR cross section are independent of the slicing cut y if y is chosen small enough. This was the case for $y \leq 10^{-3}$ in all considered cases. For $y > 10^{-3}$ we observed some small y dependence which is caused by our approximation that we neglected contributions $O(y)$ in the analytical contributions to the two–jet cross section. In the final evaluation we use $y = 10^{-3}$. Furthermore we tested that the sum of the NLO direct and the LO single resolved cross section

is independent of the factorization scale M. The same test was performed for the sum of the NLO single resolved and the LO double resolved cross section. These tests were done for the one– and two–jet cross sections separately. Similar checks have been reported for the one–jet photoproduction cross section [16].

The input for our calculation is as follows. For the DR and RR cross sections we need the parton distributions, $F_{i/\gamma}$, in the photon. We have chosen the NLO set of Glück, Reya and Vogt (GRV) in the $\overline{\rm MS}$ scheme [5]. This means that the DD, DR and RR cross sections must also be calculated with the $\overline{\rm MS}$ subtraction. We choose all scales $\mu = M = p_T$ and calculate $\alpha_s(\mu)$ from the two–loop formula with $N_f = 5$ massless flavours with $\Lambda^{(5)}_{\overline{\rm MS}} = 0.130\,GeV$ equal to the Λ value of the NLO GRV photon structure function. The charm and bottom quarks are treated also as light flavours with the boundary condition that the charm (bottom) contend of the photon vanishes for $M^2 \leq m_c^2(m_b^2)$ ($m_c = 1.5\,GeV$, $m_b = 5\,GeV$). We do not apply a special cut on the energy fractions x_a and x_b in (2) but integrate from $x_{a,\rm min}$ and $x_{b,\rm min}$ to 1, where $x_{a,\rm min}$ and $x_{b,\rm min}$ are given by kinematics (see (5)).

In the following we show results for the three different c.m. energies: (i) LEP1 with $\sqrt{S} = 90\,GeV$ and $\theta_c = 3^\circ$ in the photon spectrum in (1), (ii) LEP2 with $\sqrt{S} = 175\,GeV$ and $\theta_c = 30\,mrad$ and (iii) NLC in the TESLA design with $\sqrt{S} = 500\,GeV$ and the photon spectra given by the sum of the WWA spectrum in (1) with $\theta_c = 175\,mrad$ and the beamstrahlung spectrum given in [17] with parameters $\Upsilon_{\rm eff} = 0.039$ and $\sigma_z = 0.5\,mm$ [18]. (See [19] for the impact of various collider options.)

First we show the inclusive one–jet cross sections $\mathrm{d}^2\sigma/\mathrm{d}p_T\mathrm{d}\eta$ for the three machines. In Fig. 4 this cross section is plotted as a function of p_T for rapidity $\eta = 0$, where this cross section is maximal. Only the NLO predictions are plotted for the DD, DR and RR cross sections and for the sum of all contributions. Below $p_T = 5\,GeV$ the RR component is dominant whereas for the larger p_T the DD cross section gives the largest contribution. At $p_T = 5\,GeV$ the DD and RR cross sections are equal. Above $p_T = 10\,GeV$ the DR cross section is larger than the RR cross section. The rapidity distribution at $p_T = 5\,GeV$ is shown in Fig. 5, again for the three components and for the sum. The slight variations in the RR curve are caused by the limited accuracy of the numerical integrations. All three cross sections must be symmetric at $\eta = 0$, where they exhibit a rather broad plateau. The same distributions, i.e. $\mathrm{d}^2\sigma/\mathrm{d}p_T\mathrm{d}\eta$ for $\eta = 0$ and $\mathrm{d}^2\sigma/\mathrm{d}p_T\mathrm{d}\eta$ for $p_T = 10\,GeV$ are shown in Fig. 6 and 7 for LEP2. The qualitative behaviour of the one–jet cross sections is similar. Due to the larger c.m. energy the cross sections for LEP2 are larger than for LEP1. The RR contribution is more significant now. The DD distribution crosses the RR distribution at larger p_T than in the LEP1 case. The rapidity distribution at $p_T = 10\,GeV$ looks very similar to that in Fig. 5. At this p_T value all three components make significant contributions to the total sum. In the NLC case the pattern is somewhat different as can be seen in Fig. 8 and 9. Due to the further increase of the c.m. energy the cross section is increased by an order of magnitude as compared to the LEP2 cross section. The hierarchy between the DD, DR and RR components has changed somewhat. The RR cross sections lie for $p_T > 5\,GeV$ below the DD and DR cross sections. All three components cross each other below $p_T = 5\,GeV$, where RR starts to dominate. Above $p_T = 5\,GeV$ the p_T distribution is dominated by the DD component. The total rapidity distribution at $p_T = 10\,GeV$ is less flat around $\eta = 0$. This originates from the DD and DR part. The DD part has the steepest behaviour towards the kinematic boundaries. The different functional behaviour of $\mathrm{d}\sigma/\mathrm{d}p_T$ and $\mathrm{d}\sigma/\mathrm{d}\eta$ in Fig. 8 and 9 as compared to the cross sections for LEP2 comes from the changed photon spectra which is now a superposition of the WWA and the beamstrahlung spectrum. The rapidity distribution for the NLC looks similar to the results obtained recently for charm

quark production in two–photon collisions [20]. However, the difference between the LEP2 and NLC rapidity distributions is even more drastic for heavy quark production than in Fig. 7 and 9. By comparing with the LO one–jet cross section, where the same photon structure function and the same α_s as in the NLO cross section is used we obtained the k factors for the RR contributions. They are $k = 1.85$, 1.90 and 1.90 for the three cases LEP1, LEP2 and NLC. We shall use these k factors for correcting the LO RR predictions of the two–jet cross sections.

Next we consider the results on inclusive two–jet production which will be shown in the following figures for the LEP2 case. In Fig. 10, 11 and 12, we present $\mathrm{d}^3\sigma/\mathrm{d}p_T\mathrm{d}\eta_1\mathrm{d}\eta_2$ as a function of p_{T_1} for $\eta_1 = 0$ and various choices of $\eta_2 = 0$, 1, 2. Here, p_{T_1} and η_1 are the transverse momentum and the rapidity of the so–called trigger jet. η_2 is the rapidity of the second jet, so that p_{T_1} and p_{T_2} are the two highest transverse momenta of the three–jet configuration. For exactly two jets in the final state, we have $p_{T_1} = p_{T_2}$. In Fig. 11 and 12, we can see how the cross section decreases when η_2 is chosen away from the maximum region at $\eta_2 = 0$. In particular the RR component becomes more important for increasing p_T when η_2 increases. $\eta_1 = 0$ is always kept fixed. Comparing the cross sections in Fig. 10 and 11 we see that the sum of the three components hardly changes when $\eta_2 = 1$ instead of $\eta_2 = 0$, although the relation of the DD, DR and RR cross sections is different in the two cases. We have studied the inclusive two–jet cross section also as a function of η_1 and η_2 for fixed p_{T_1}. As an example, we show for LEP2 the two–dimensional distribution $\mathrm{d}^3\sigma/\mathrm{d}p_T\mathrm{d}\eta_1\mathrm{d}\eta_2$ for $p_{T_1} = 10\,GeV$ in form of a lego–plot in the intervals η_1, $\eta_2 \in [-3.0, 3.0]$. The cross sections for the DD, DR and RR contributions and for the sum are shown separately. The DR cross section contains both contributions with the resolved photon at the upper or the lower vertex. If they are considered separately we checked that they are symmetric for $\eta_1 \leftrightarrow \eta_2$.

For the NLC case we present only $\mathrm{d}^3\sigma/\mathrm{d}p_T\mathrm{d}\eta_1\mathrm{d}\eta_2$ as a function of p_{T_1} for $\eta_1 = \eta_2 = 0$ where the two–jet cross section is maximal. This is shown in Fig. 14. Comparing with the corresponding cross section for LEP2 in Fig. 10 we notice the increase of the cross section by more than a factor 10 and that the RR component is somewhat more significant also for larger p_T. The cross section $\mathrm{d}^3\sigma/\mathrm{d}p_T\mathrm{d}\eta_1\mathrm{d}\eta_2$ as a function of η_2 for $p_{T_1} = 10\,GeV$ and $\eta_1 = 0$ is presented in Fig. 15 for the three components DD, DR, RR and the sum. Only the RR cross section is rather flat near the maximum $\eta_2 = 0$. The other components are much steeper away from $\eta_2 = 0$ as it is the case also in the sum similar to the one–jet cross section shown in Fig. 9.

It is clear that many more distributions or partially integrated cross sections using other two–jet variables can be calculated with the phase space slicing method. So, for example, one could study kinematic regions where either the DD or the RR cross section is enhanced, as has been done for two–jet production in γp processes [10] by making cuts in x_γ, the fraction of the photon energy participating in the hard scattering process. Other interesting topics are the cone dependence of the inclusive cross sections or the study of the invariant mass distribution of the two jets for different rapidities or the angular distribution of the two jets to test the parton–parton scattering dynamics in a different way.

5 Summary and Conclusions

Various inclusive one– and two–jet cross sections have been calculated for the direct, single resolved and double resolved contributions as a function of p_T and jet rapidities in NLO. For the double resolved two–jet cross section the NLO corrections are estimated with a k factor taken from the inclusive one–jet cross section. For the direct and single resolved components all NLO corrections are fully evaluated. Infrared and collinear singularities are cancelled with

the phase space slicing method using an invariant mass cut–off. This method is particularly useful for incorporating cuts on the final state and for obtaining results with different choices of jet algorithms. Analytical formulas for the different contributions giving the dependence on the slicing parameter are derived for the direct contribution. The same results for the single resolved contribution are taken from the corresponding calculation of jet production in γp processes [10].

Numerical results for the inclusive one–jet and two–jet cross sections in three energy ranges corresponding to LEP1, LEP2 and NLC have been presented. In the NLC case we have calculated the photon spectra from a superimposition of bremsstrahlung and beamstrahlung spectra. For this case the photon spectra lead to quite different rapidity distributions as compared to LEP1 and LEP2 where we have only the bremsstrahlung spectrum. The hierarchy of direct, single and double resolved cross section is very similar for the three machines. The RR component dominates only for rather small $p_T \leq 5\,GeV$ in all cases. For larger p_T the direct contribution is dominant.

Since our results have been successfully tested already at smaller energies by comparing with one– and two–jet measurements of the TOPAZ and AMY collaborations we are confident that our results are also reliable for the larger energies achievable at LEP2 and NLC.

A Virtual Correction

$$
\begin{aligned}
V_\gamma(s,t,u) &= \left[-\frac{2}{\epsilon^2}-\frac{3}{\epsilon}+\frac{2\pi^2}{3}-7+\ln^2\frac{-t}{s}+\ln^2\frac{-u}{s}\right] T_\gamma^{(\epsilon)}(s,t,u) \\
&\quad +2\ln\frac{-t}{s}+2\ln\frac{-u}{s}+3\frac{u}{t}\ln\frac{-t}{s}+3\frac{t}{u}\ln\frac{-u}{s} \\
&\quad +\left(2+\frac{u}{t}\right)\ln^2\frac{-u}{s}+\left(2+\frac{t}{u}\right)\ln^2\frac{-t}{s}
\end{aligned} \tag{49}
$$

B Final State Correction

$$
F_\gamma(s,t,u) = \left[\frac{2}{\epsilon^2}+\frac{3}{\epsilon}+7-2\ln^2 y_F-3\ln y_F\right] T_\gamma^{(\epsilon)}(s,t,u) \tag{50}
$$

C Initial State Correction

$$
I_\gamma(z;s,t,u) = \left[-\frac{1}{\epsilon}\frac{1}{N_C Q^2}P_{q\leftarrow\gamma}(z)+1+\ln\left(\frac{y_I(1-z)}{z}\right)\left(2z^2-2z+1\right)\right] T_q^{(\epsilon)}(s,t,u) \tag{51}
$$

Here one needs the Altarelli–Parisi splitting function for the process photon $\rightarrow$ quark, which is

$$
P_{q\leftarrow\gamma}(z) = N_C Q^2\left[2z^2+2z+1\right] \tag{52}
$$

References

[1] T. Kleinwort, G. Kramer, DESY 95–172, September 1995.

[2] H. Hayashii et al., TOPAZ Collaboration, Phys. Lett. B314 (1993) 149.

[3] B. J. Kim et al., AMY Collaboration, Phys. Lett. B325 (1994) 248.

[4] M. Drees, R. M. Godbole, Nucl. Phys. B339 (1990) 355.

[5] M. Glück, E. Reya, A. Vogt, Phys. Rev. D45 (1992) 3986, Phys. Rev. D46 (1992) 1973.

[6] L. E. Gordon, J. K. Storrow, Z. Phys. C56 (1992) 307;
P. Aurenche, P. Chiapetta, M. Fontannaz, J.–Ph. Guillet, E. Pilon, Z. Phys. C56 (1992) 589.

[7] P. Aurenche, J.–Ph. Guillet, M. Fontannaz, Y. Shimizu, J. Fujimoto, K. Kato, Progr. Theor. Phys. 92 (1994) 175;
P. Aurenche, J.–Ph. Guillet, M. Fontannaz, Y. Shimizu, J. Fujimoto, K. Kato, Proc. of the Workshop on Two–Photon Physics at LEP and HERA, Lund, Eds. G. Jarlskog and L. Jönsson, Lund Univ., 1994, p. 269.

[8] L. E. Gordon, Nucl. Phys. B 419 (1994) 25.

[9] F. A. Berends, Z. Kunszt, R. Gastmans, Nucl. Phys. B 182 (1981) 397;
I. Kang, Oxford University preprint 50/82 (1982).

[10] M. Klasen, G. Kramer, Phys. Lett. B366 (1996) 385; DESY 95–226, December 1995, to be published in Z. Phys. C.

[11] G. Kramer, S.G. Salesch Z. Phys. C61 (1994) 277;
S. G. Salesch, DESY 93–196, December 1993.

[12] S. Frixione, M.L. Mangano, P. Nason, G. Ridolfi, Phys. Lett. B 319 (1993) 339.

[13] P. Aurenche, R. Baier, A. Douiri, M. Fontannaz, D. Schiff, Z. Phys. C27 (1985), 423.

[14] J.E. Huth et al., Proc. of the 1990 DPF Summer Study on High Energy Physics, Snowmass, Colorado, edited by E.L. Berger, World Scientific, Singapore, 1992, p. 134.

[15] S.D. Ellis, Z. Kunszt, D.E. Soper, Phys. Rev. Lett. 62 (1989) 726,
Phys. Rev. D 40 (1989) 2188, Phys. Lett. Rev. 64 (1990) 2121.

[16] D. Bödecker, G. Kramer, S.G. Salesch, Z. Phys. C63 (1994) 471.

[17] T. Barklow, P. Chen, W. Kozanecki, in *Proceeding of the Workshop on* e^+e^- *Collisions at* $500\,GeV$*: The Physics Potential,* edited by P.M. Zerwas, DESY Orange Report No. 92–123B (1992) p. 845;
P. Chen, T. Barklow, M. Peskin, Phys. Rev. D49 (1994) 3209.

[18] D. Schulte, private communication.

[19] M. Drees, R.M. Godbole, Z. Phys. C59 (1993) 591.

[20] M. Cacciari, M. Greco, B.A. Kniehl, M. Krämer, G. Kramer, M. Spira, DESY 95–205, FNT/T–95–28, LNF–95/059(P), MPI/PhT/95–113, to be published in Nucl. Phys. B.

4 Figure Captions

Fig. 1: The three body diagrams for $\gamma\gamma \to q\bar{q}g$.

Fig. 2: Three body diagrams with final and initial state singularities.

Fig. 3: Kinematic diagram for the three–body final state defining the angles in the c.m. system of partons p_1 and p_2.

Fig. 4: NLO inclusive one–jet cross section $\mathrm{d}^2\sigma/\mathrm{d}p_T\mathrm{d}\eta$ as a function of p_T at $\eta = 0$ for direct (DD), single resolved (DR) and double resolved (RR) contributions and for the sum of all components. LEP1 photon spectra, $\sqrt{S} = 90\,GeV$.

Fig. 5: NLO inclusive one–jet cross section as a function of η at $p_T = 5\,GeV$ and for DD, DR, RR and the sum. LEP1 photon spectra, $\sqrt{S} = 90\,GeV$.

Fig. 6: Same as Fig. 4. LEP2 photon spectra, $\sqrt{S} = 175\,GeV$.

Fig. 7: Same as Fig. 5, $p_T = 10\,GeV$. LEP2 photon spectra, $\sqrt{S} = 175\,GeV$

Fig. 8: Same as Fig. 4. NLC–TESLA photon spectra. $\sqrt{S} = 500\,GeV$.

Fig. 9: Same as Fig. 5, $p_T = 10\,GeV$. NLC–TESLA photon spectra. $\sqrt{S} = 500\,GeV$.

Fig. 10: NLO inclusive two–jet cross section as a function of p_T for $\eta_1 = \eta_2 = 0$ for direct (DD), single resolved (DR), double resolved (RR) and sum. LEP2 photon spectra. $\sqrt{S} = 175\,GeV$. RR component estimated with k factor.

Fig. 11: Same as Fig. 10 for $\eta_1 = 0$, $\eta_2 = 1$.

Fig. 12: Same as Fig. 10 for $\eta_1 = 0$, $\eta_2 = 2$.

Fig. 13: NLO triple differential cross section $\mathrm{d}^3\sigma/\mathrm{d}p_T\mathrm{d}\eta_1\mathrm{d}\eta_2$ for $p_T = 10\,GeV$ as a function of η_1 and η_2 for DD, DR, RR components and the sum. LEP2 photon spectra. $\sqrt{S} = 175\,GeV$.

Fig. 14: Same as Fig. 10. NLC–TESLA photon spectra. $\sqrt{S} = 500\,GeV$.

Fig. 15: NLO inclusive two–jet cross section as a function of η_2 for $p_T = 10\,GeV$ and $\eta_1 = 0$. NLC–TESLA photon spectra. $\sqrt{S} = 500\,GeV$.

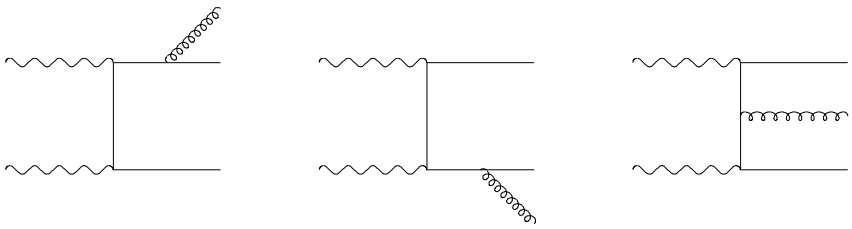

Figure 1:

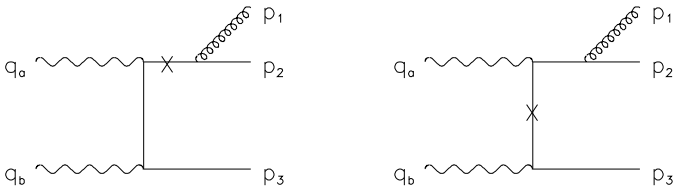

Figure 2:

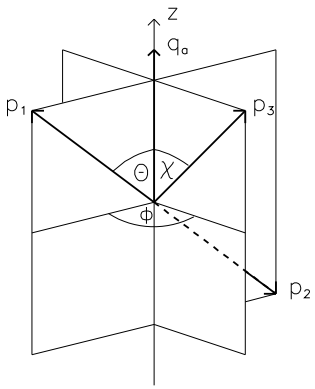

Figure 3:

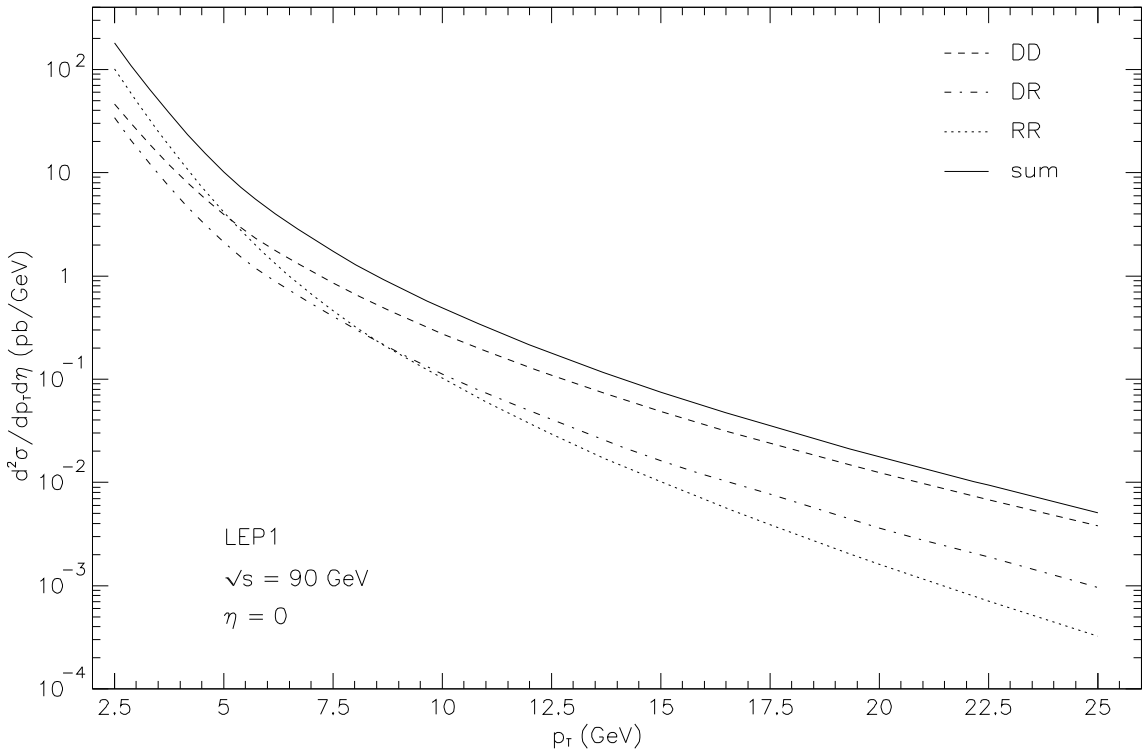

Figure 4:

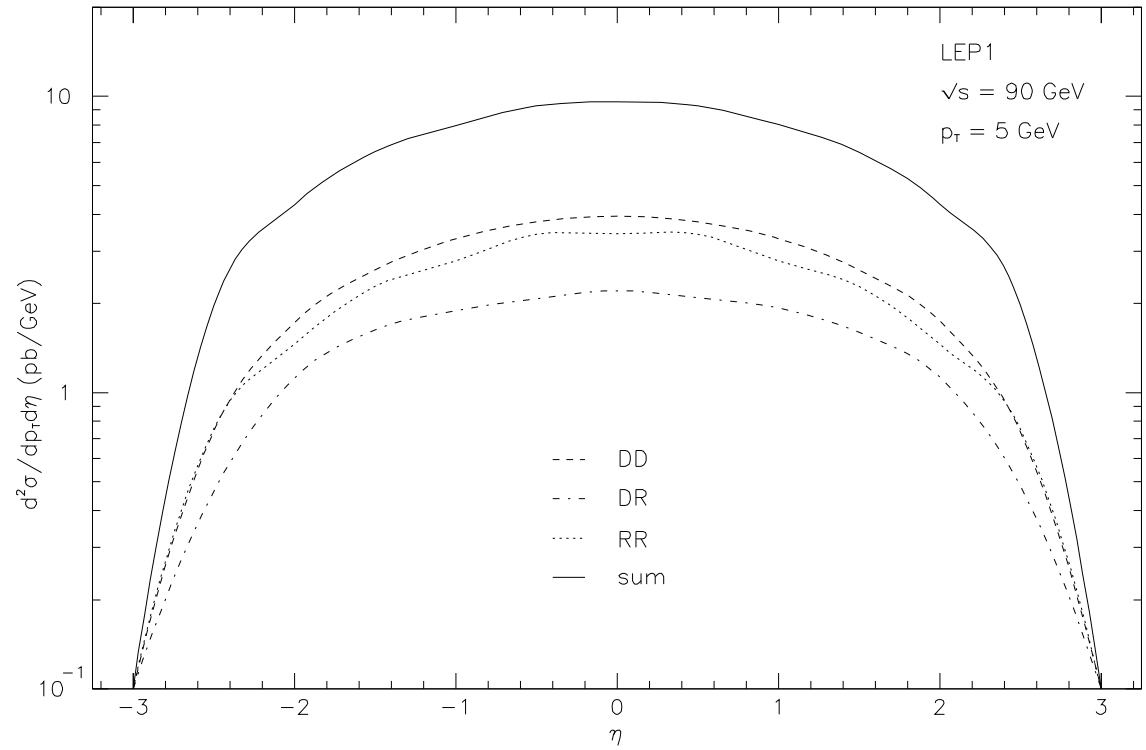

Figure 5:

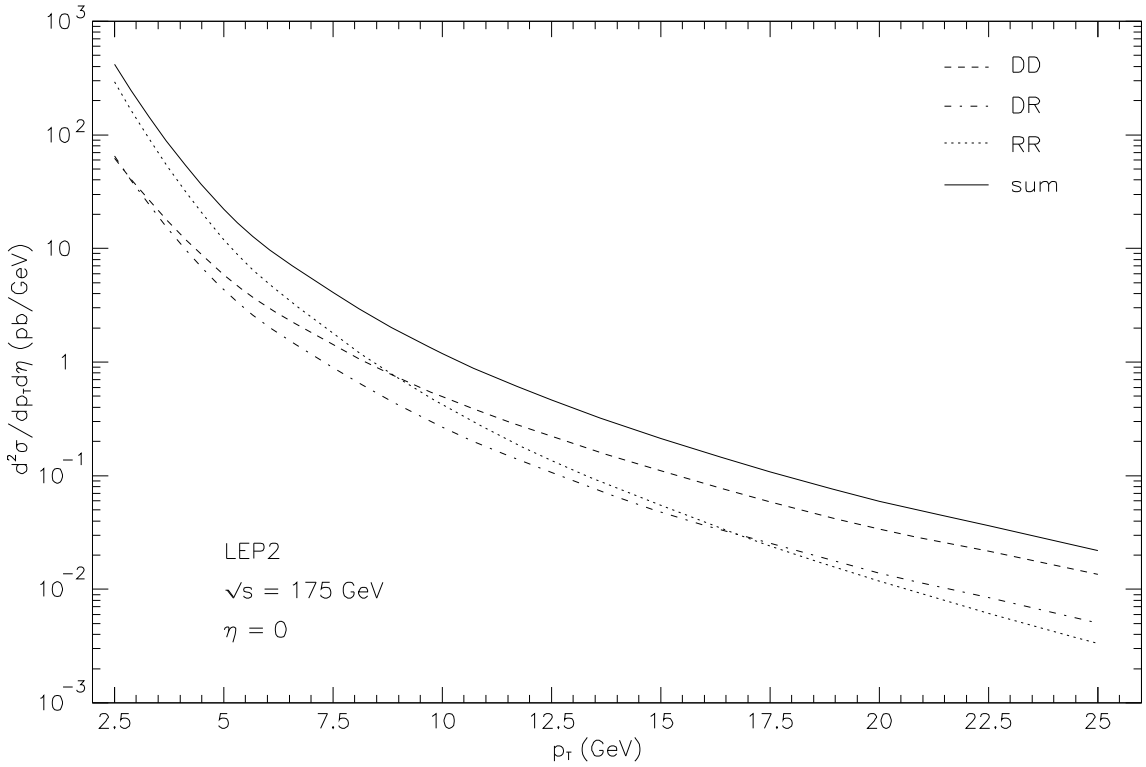

Figure 6:

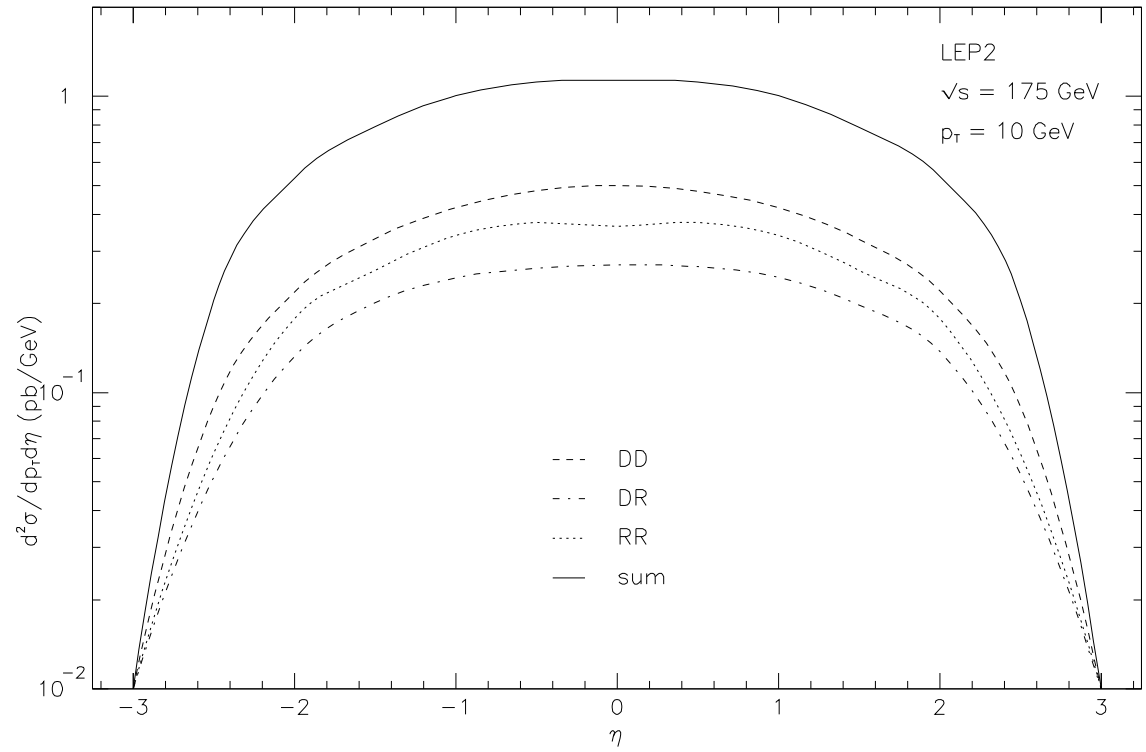

Figure 7:

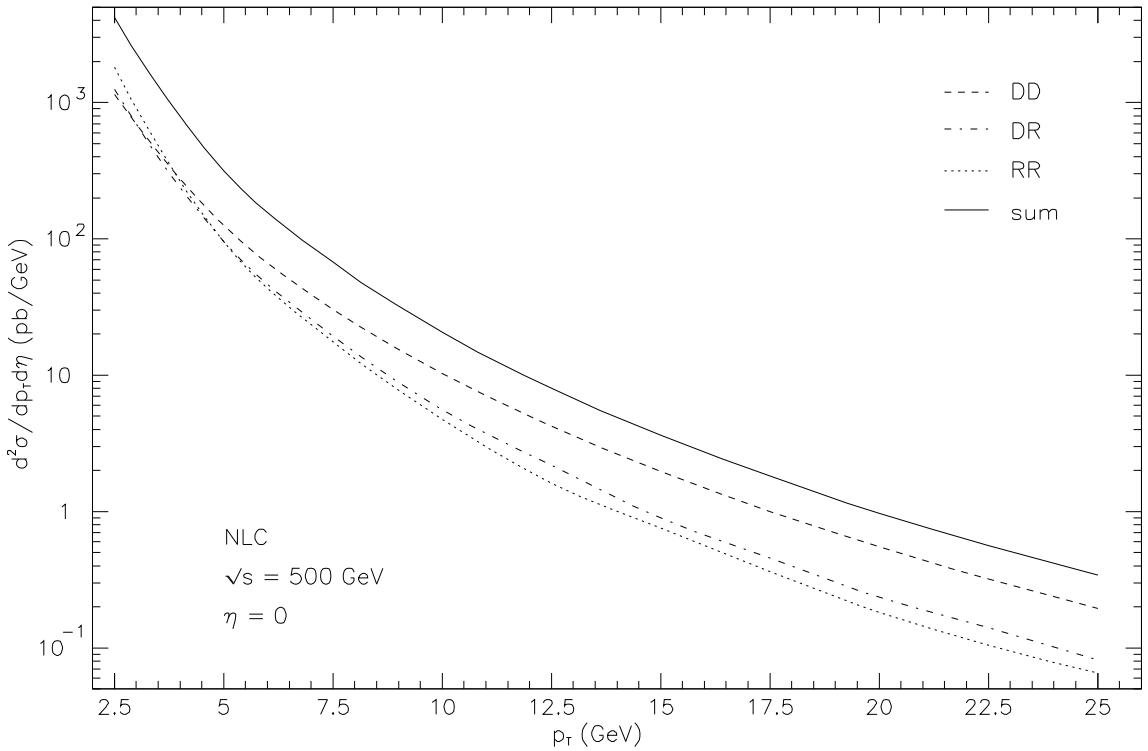

Figure 8:

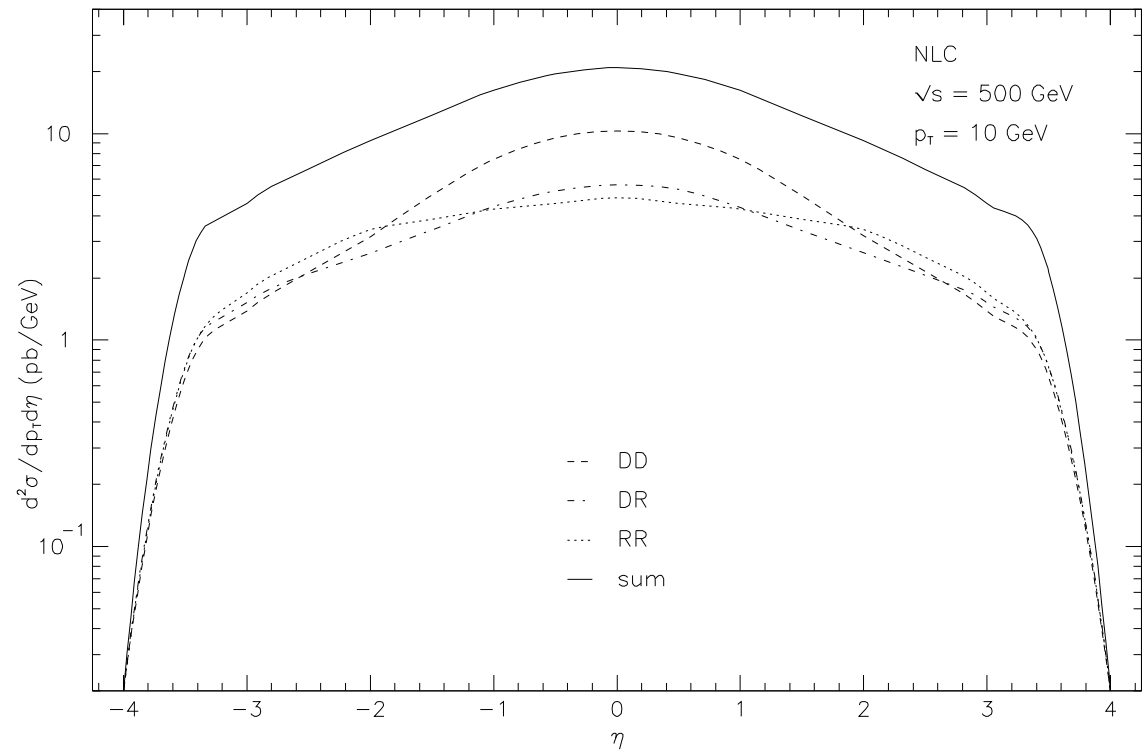

Figure 9:

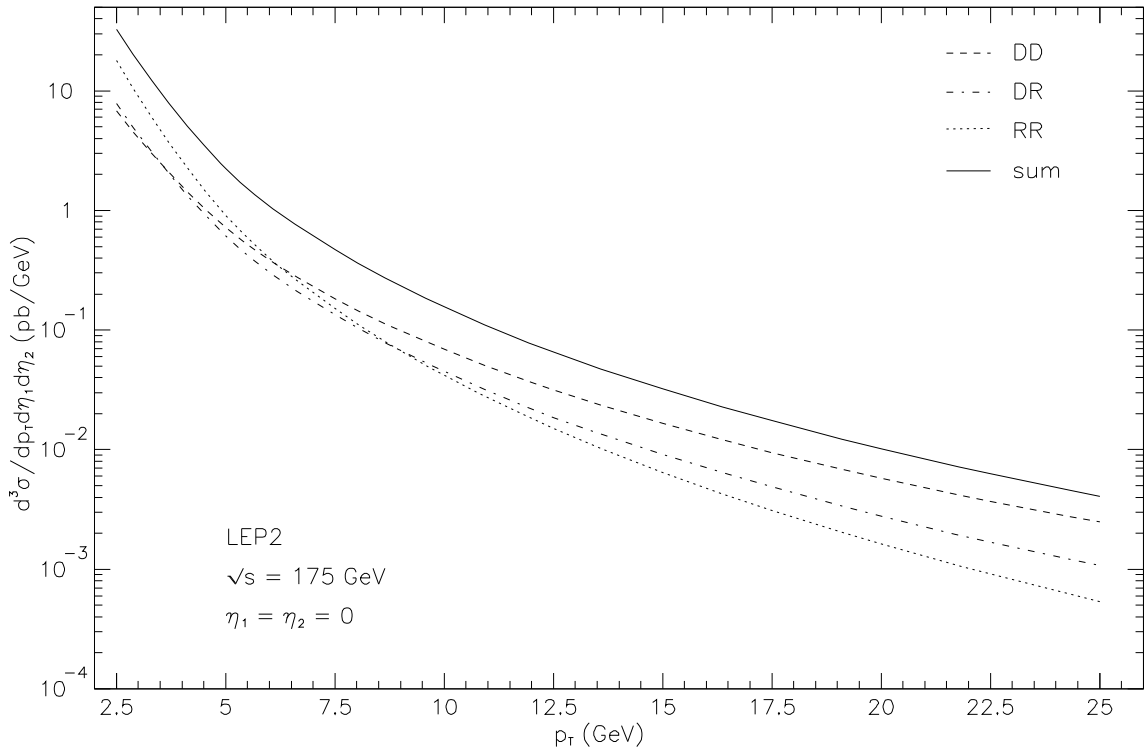

Figure 10:

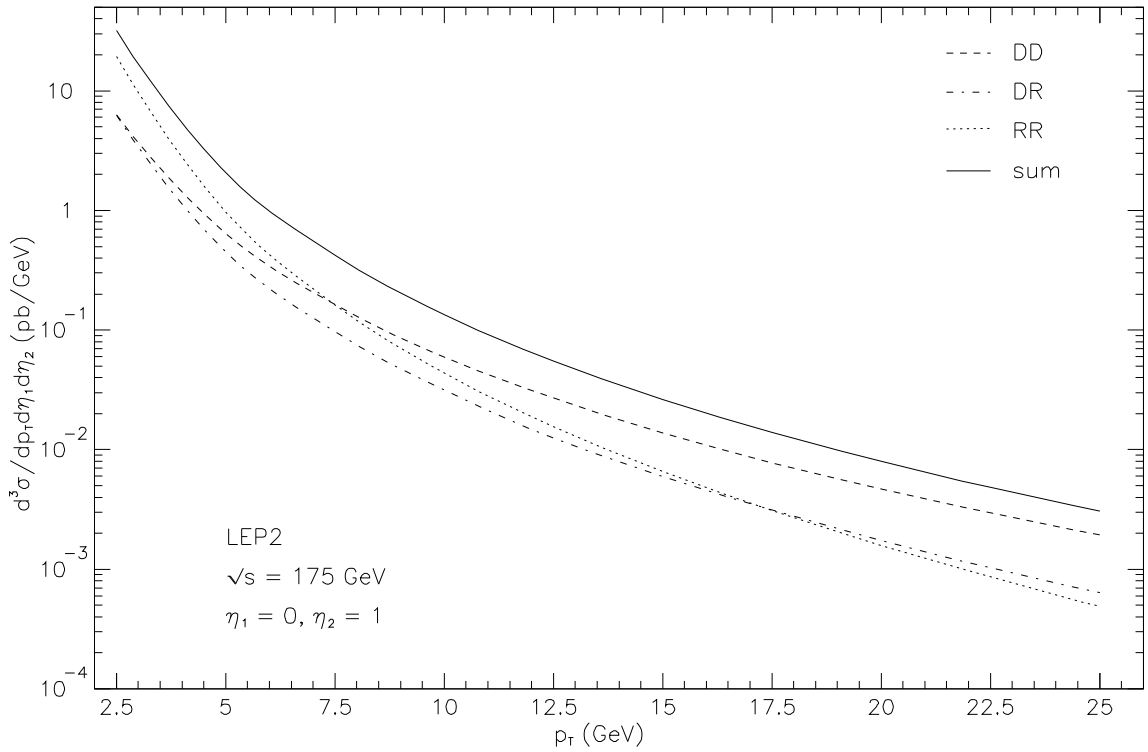

Figure 11:

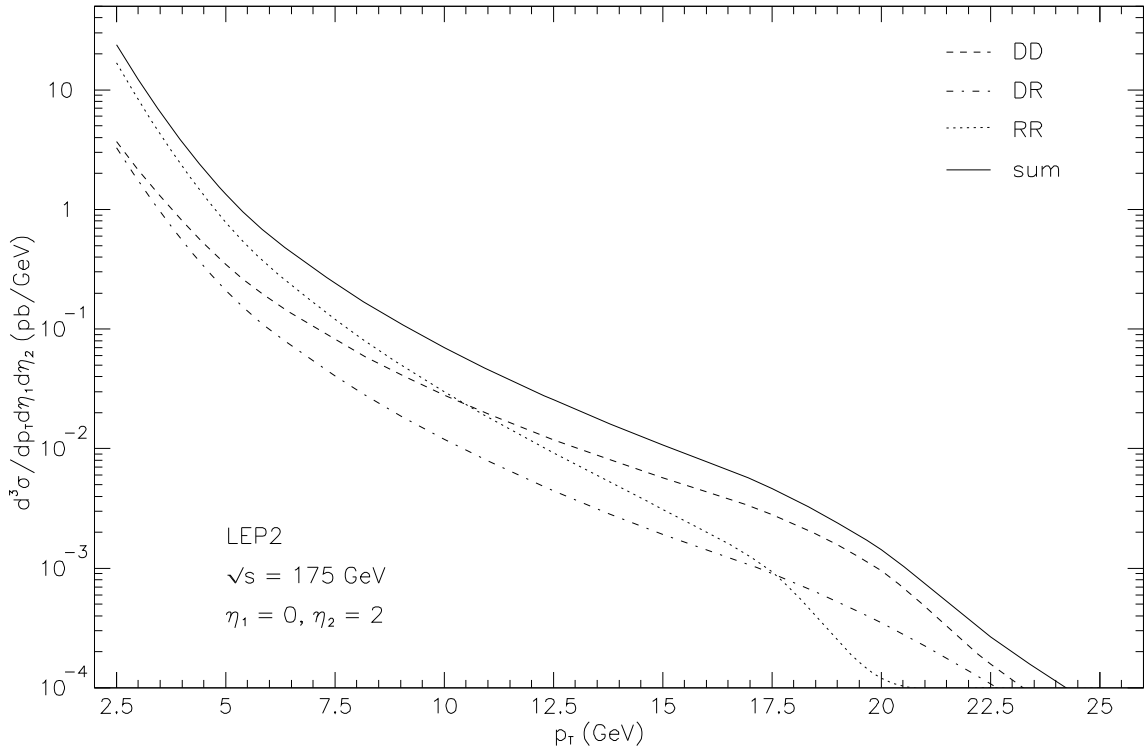
DD
DR
RR
sum
LEP2
√s = 175 GeV
η₁ = 0, η₂ = 2
d³σ/dp_T dη₁ dη₂ (pb/GeV)
p_T (GeV)
10
1
10⁻¹
10⁻²
10⁻³
10⁻⁴
2.5
5
7.5
10
12.5
15
17.5
20
22.5
25

Figure 12:

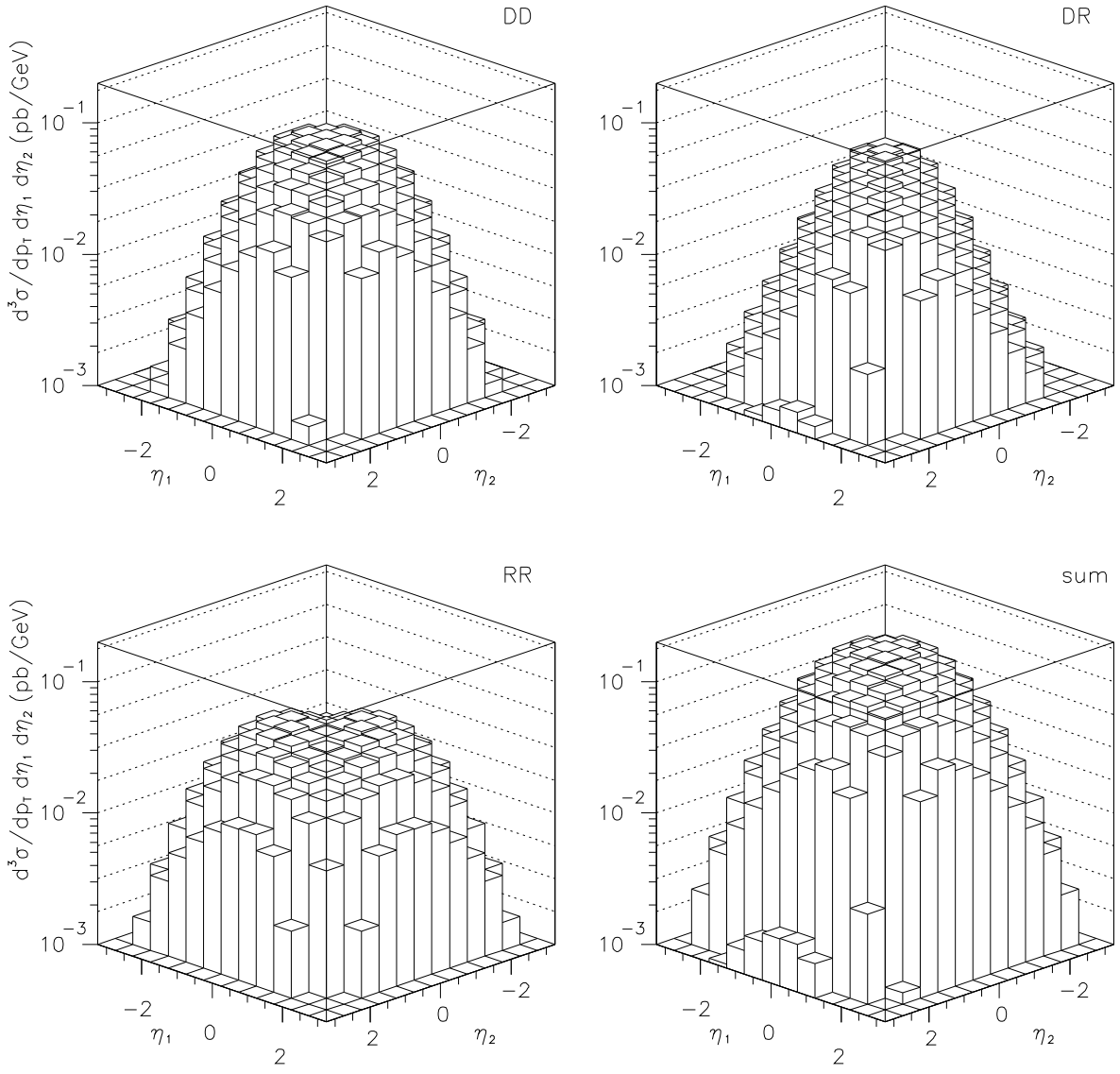
DD
DR
RR
sum
$d^3\sigma/dp_T\,d\eta_1\,d\eta_2$ (pb/GeV)
10^{-1}
10^{-2}
10^{-3}
η_1
η_2
−2
0
2

Figure 13:

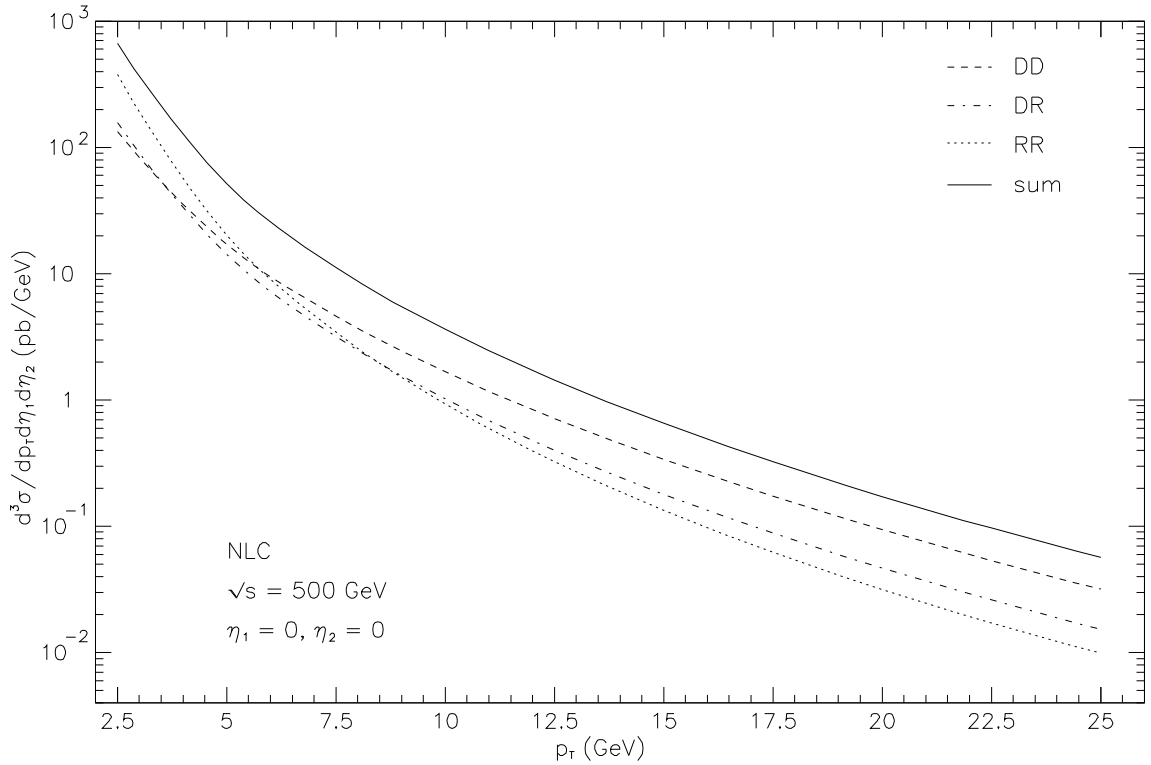

Figure 14:

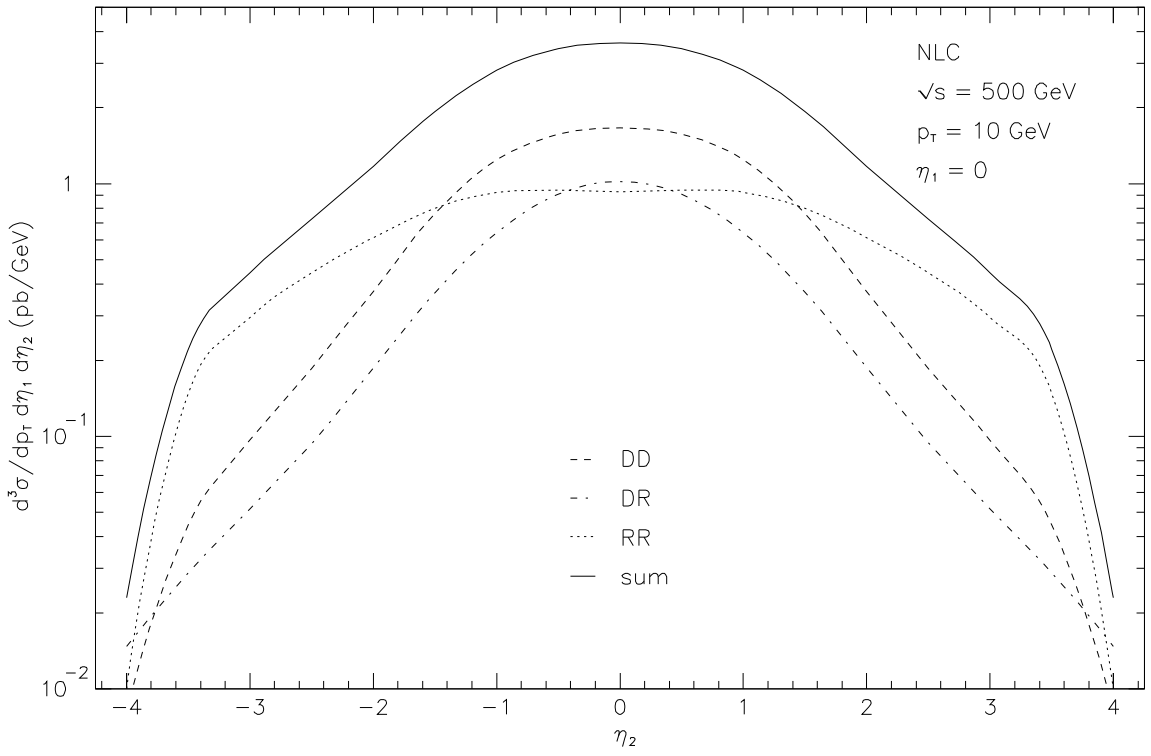

Figure 15: